Applied Surface Science 563 (2021) 150276

Contents lists available at ScienceDirect

Applied Surface Science

journal homepage: www.elsevier.com/locate/apsusc

Full Length Article

Switchable electric polarization of phosphorene in mixed dimensional van der Waals heterostructure

Fei Wang [a,*], Zhuang Ma [a,b], Yuting Wei [a], Pu Huang [b], Xiuwen Zhang [b,*]

[a] International Laboratory for Quantum Functional Materials of Henan, School of Physics and Microelectronics, Zhengzhou University, Zhengzhou 450001, China
[b] Key Laboratory of Optoelectronic Devices and Systems of Ministry of Education and Guangdong Province, College of Physics and Optoelectronic Engineering, Shenzhen University, Shenzhen 518060, China

ARTICLE INFO

Keywords:
Phosphorene
Polarization
First-principles calculations

ABSTRACT

Switchable electric polarization in semiconductors has promising applications in nanoelectronic and optoelectronic devices. Here, we propose a type of two-dimensional (2D) polarization switchable by angstrom-scale position shifts of phosphorene on PbTe. As a homo-atomic analogue to the 2D ferroelectric monolayer GeS, non-ferroelectric phosphorene acquires in-plane electric polarization by breaking the in-plane and out-of-plane symmetry via proximity of phosphorene to PbTe compound in the mixed dimensional vertical P/PbTe heterostructure. We demonstrate via first-principles calculations the asymmetric charge distribution on the two P sublattices in phosphorene, rendered by the alternative cation and anion chains in PbTe substrate that breaks the glide reflection symmetry and inversion symmetry of phosphorene, leading to the in-plane polarization. It is found that the in-plane polarization in phosphorene can be significantly modulated by interlayer strain and external electric field. More interestingly, the in-plane electric polarization switches sign when phosphorene shifts on PbTe substrate by an interval between the cation and anion chains with a low transition barrier of a few meV/P-atom. Our study demonstrates that the switching of 2D in-plane polarization via spatial shifting in phosphorene-based van der Waals heterostructures, with promising applications in 2D polarization functionalized nanoelectronic and optoelectronic devices.

1. Introduction

Ferroelectric materials have been attracting lots of attention due to their intriguing physical properties and critical applications such as ferroelectric capacitors, non-volatile memories, ferroelectric tunnel junctions, and sensors [1,2]. Recently, two-dimensional ferroelectric atomic crystals have attracted much attention due to their intriguing physical properties and potential applications in nanoelectronic devices [3–8]. Ferroelectricity as well as ferroelasticity were predicted in monolayer group IV monochalcogenides [9–11]. Especially, robust in-plane ferroelectricity was observed in 2D SnTe [12], enabling the miniaturization of ferroelectric devices. These monolayer IV-VI crystals are daughter structures of the mono-atomic phosphorene [13,14], with the two P (group V) sublattices separately into the IV and VI sublattices, respectively, analogous to the zincblende daughter structure of diamond lattice. Unlike the mono-atomic crystal graphene with vanishing band gap [15,16], phosphorene exhibits a moderate direct band gap of 1.73 eV [17], suitable for electronic and optoelectronic applications. Furthermore, phosphorene has high hole mobilities exceeding 1000 $cm^2 V^{-1} s^{-1}$ and highly anisotropic electronic structure [18]. Analogous to the Dresselhaus versus hidden Dresselhaus spin effects in zincblende versus diamond materials [19], phosphorene with the two inversion-symmetric P sublattices, possesses compensated local electric polarization as opposed to the ferroelectricity in IV-VI monolayers. Modulation phosphorene by external perturbation such as electric field could significantly extend its application in nanoelectronics devices. It was predicted that specific phosphorene nanoribbons with an odd number of P atoms in the in-plane transverse direction possess in-plane ferroelectricity along the longitudinal direction in the presence of vertical electric field, whereas for the nanoribbons with even number of P in the transverse direction, the ferroelectricity is absent [20]. Such ferroelectricity is also absent in 2D phosphorene under vertical electric field due to the presence of the glide reflection symmetry between the two P sublattices [20]. It is thus intriguing to find an approach to induce electric polarization and the associated materials' properties in 2D phosphorene.

Stacking two or more layers of different 2D materials has led to rich

* Corresponding authors.
E-mail addresses: wfei@zzu.edu.cn (F. Wang), xiuwenzhang@szu.edu.cn (X. Zhang).

https://doi.org/10.1016/j.apsusc.2021.150276
Received 19 January 2021; Received in revised form 28 May 2021; Accepted 30 May 2021
Available online 2 June 2021

2D electronic systems for studying novel quantum phenomena at the interface [21–29]. The combination of van der Waals (vdW) and layered materials combines structural and electronic diversity, opening up new avenues for basic scientific research and device application [30–33]. However, there are several challenges in 2D materials that limit the development and application of 2D vdW heterostructures, such as the limitation in modulation capacity and high experimental cost. An alternative approach is constructing mixed dimensional vdW heterostructures, e.g. a 2D layer vdW interact with a bulk material, which have a few outstanding advantages, such as higher chemical and thermal stability and facile experiment preparation [30,33]. Studies have shown that most mixed dimensional vdW heterostructures are more thermally and chemically stable than 2D vdW heterostructures [34–36].

Here, we propose using a mixed dimensional P/PbTe vdW heterostructure to induce in-plane electric polarization in phosphorene. First-principles calculations show that the intrinsic electronic properties of phosphorene and PbTe are preserved in the vdW heterostructure. Calculated results show that the two P sublattices that are inversion symmetric in free standing phosphorene, possess asymmetric charge distribution in the mixed dimensional vdW heterostructure, rendered by the cation/anion chains in PbTe substrate, that breaks the inversion symmetry, in-plane rotational symmetries, and the glide reflection symmetry of phosphorene and induces an in-plane electric polarization. It is further found that the in-plane electric polarization of phosphorene can be significantly modulated by interlayer strain and external electric field. More interestingly, the in-plane electric polarization switches sign when the phosphorene slides on the PbTe substrate by an interval between cation and anion chains, in angstrom-scale. Our study demonstrates that the switchable in-plane electric polarization in mixed dimensional vdW heterostructures can be realized via atomic scale spatial shifting, which may have broad applications in low-dimensional materials and vdW heterostructures.

2. Computational details

All calculations are done by the plane-wave pseudopotential as implemented in the Vienna ab initio simulation package (VASP) software package [37,38] based on density functional theory. The frozen-core projected augmented wave (PAW) pseudopotentials are used to deal with the interaction between ions and electrons. The exchange–correlation functional is described by the Perdew-Burke-Ernzerhof (PBE) parameterization [39–41]. After testing, the plane wave cutoff energy was set to 400 eV in this work, which is accurate enough. In the structural optimization, a $7 \times 7 \times 1$ k-point grid sampling in the Brillouin zone (BZ) was used [42] and the total energy and force on each atom converge to 10^{-5} eV and 0.01 eV/Å, respectively. In the P/PbTe vdW heterostructure, a vacuum layer with a thickness greater than 20 Å in the z direction was set to avoid layer-to-layer interactions. In the calculation of heterostructures, three layers of PbTe are considered, with the bottom layer of PbTe fixed to mimic bulk material, and the top two layers of PbTe allowed to relax. In vertical compressive strain study, the z coordinates in the bottom layer of phosphorene and the top layer of PbTe are fixed, to tune the magnitude of stain. For optimization and calculation of the stack structure, a van der Waals correction that considers the interaction between layers has been introduced. In addition, the spin-orbit coupling (SOC) effect is included in the self-consistent calculation of the electronic structure to verify its role in the heterostructure. For phonon spectrum calculations, we have carried out the supercell approach within the framework of force-constants method [43,44]. Real-space force constants of the supercell are calculated in the density-functional perturbation theory as implemented in the VASP code [37,38] from forces on atoms with finite atomic displacements in supercell containing $3 \times 3 \times 1$ unit cells. The phonon modes are calculated from the force constants by using the PHONOPY package [43,44].

The electric polarization of phosphorene on top of PbTe substrate is demonstrated by calculating the polarization value of the slightly distorted phosphorene structure as found in the P/PbTe vdW heterostructure based on the method of the Berry phase expressions of the modern theory of polarization [45], which showed that the electronic contribution to the difference in polarization, due to a finite adiabatic change in the Hamiltonian of a system, can be identified as a geometric quantum phase or Berry phase of the valence wave functions [46,47]. The electric polarization of phosphorene has been calculated as the difference between the reference non-polarization ideal phase and the slightly distorted structure in the P/PbTe supercell. To avoid polarization quanta, a path of 8 intermediate structures between initial and final distorted phase is used. A $5 \times 5 \times 1$ k-point grid in the BZ is used for the Berry phase polarization calculation. These parameters have been tested and can give good convergence in our polarization calculations.

3. Results and discussion

3.1. Electronic structure and electric polarization of P/PbTe heterostructure

We first analyse the property of phosphorene as compared to the ferroelectricity in IV-VI monolayers. Phosphorene has the Cmca (D_{2h}) space group and a puckered structure with strong anisotropy. In comparison to IV-VI monolayers, phosphorene possesses inversion symmetry, an in-plane rotational symmetry, and an in-plane glide reflection symmetry along the zigzag direction between the two P sublattices that correspond to the IV and VI sublattices in IV-VI, as shown in Fig. 1(a). As the above noted symmetries are broken, IV-VI monolayers are multiferroic with coupled ferroelectricity and ferroelasticity [9,10]. In phosphorene, with similar local structures as IV-VI monolayers, the local dipole fields of the P atoms compensate each other due to the high crystalline symmetries (e.g., glide reflection symmetry and inversion symmetry), leading to an non-ferroelectric structure. Analogously, IV-VI (e.g. GeS) bilayers could also possess the inversion symmetry and antiferroelectricity. In Fig. 1(b), we show the energy profiles of antiferroelectric switching as a function of step number in the climbing image nudged elastic band method [48] (NEB) plotted for phosphorene and GeS bilayer. The calculated energy barriers are 0.52 and 0.18 eV/atom for phosphorene and GeS bilayer, respectively, similar to the previously results [9,10]. The higher energy barrier in phosphorene than GeS is due to the stronger atomic bonds in phosphorene than those of GeS, which suggests that phosphorene would have rather high transition temperature.

We then attempt to induce in-plane electric polarization in phosphorene by breaking its in-plane rotational symmetry, glide reflection symmetry, and inversion symmetry to become analogous to the ferroelectric IV-VI monolayers. A vertical electric field would break the in-plane rotational symmetry and inversion symmetry, whereas leave the glide reflection symmetry intact. We then construct a mixed dimensional heterostructure between 2D phosphorene and 3D compound PbTe to break the inversion symmetry and in-plane rotational symmetry by the asymmetric vertical geometry, and to break the glide reflection symmetry by the lateral geometry of the cations and anions on the surface of PbTe substrate (see Fig. 2(a)). We select PbTe as the substrate based on the calculated geometric parameters of the monolayer phosphorene and bulk PbTe. For monolayer phosphorene, we obtain the optimized lattice constants $a = 3.30$ Å, $b = 4.62$ Å in the orthogonal structure, and P-P bond lengths of 2.24 Å and 2.27 Å, which are consistent with previous studies [49]. For bulk PbTe that belongs to face-centred cubic structure, the relaxed lattice constant is $a = b = 6.56$ Å, which also agrees well with the experimentally and theoretically reported values. In order to match the two materials with different dimensions, we constructed a 3×2 supercell of phosphorene (containing 24P atoms) and a $\sqrt{2} \times \sqrt{2}$ supercell of PbTe (containing 12 Pb and 12 Te atoms) to form a P/PbTe vdW heterostructure, as shown in Fig. 2(a). The lattice mismatch of the

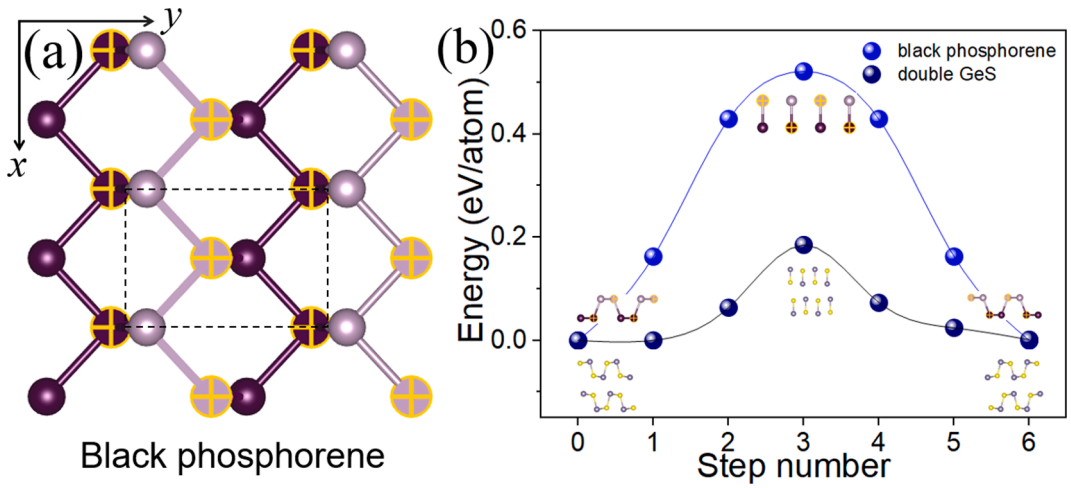

Fig. 1. (a) Crystal structures of phosphorene (top view). The dark purple and light pink spheres denote the different layers of P atoms in phosphorene. The marked (by yellow plus signs) and unmarked spheres denote the P atoms in the two P sublattices of phosphorene corresponding to the Ge and S sublattices of GeS. The dash rectangular shows the unit cell of phosphorene. (b) The energy profiles of anti-ferroelectric switching as a function of step number in the NEB computation are plotted for phosphorene and GeS bilayer. Inset: side views of phosphorene and GeS bilayer. The dark grey and bright yellow spheres are Ge and S atoms in GeS. (For interpretation of the references to colour in this figure legend, the reader is referred to the web version of this article.)

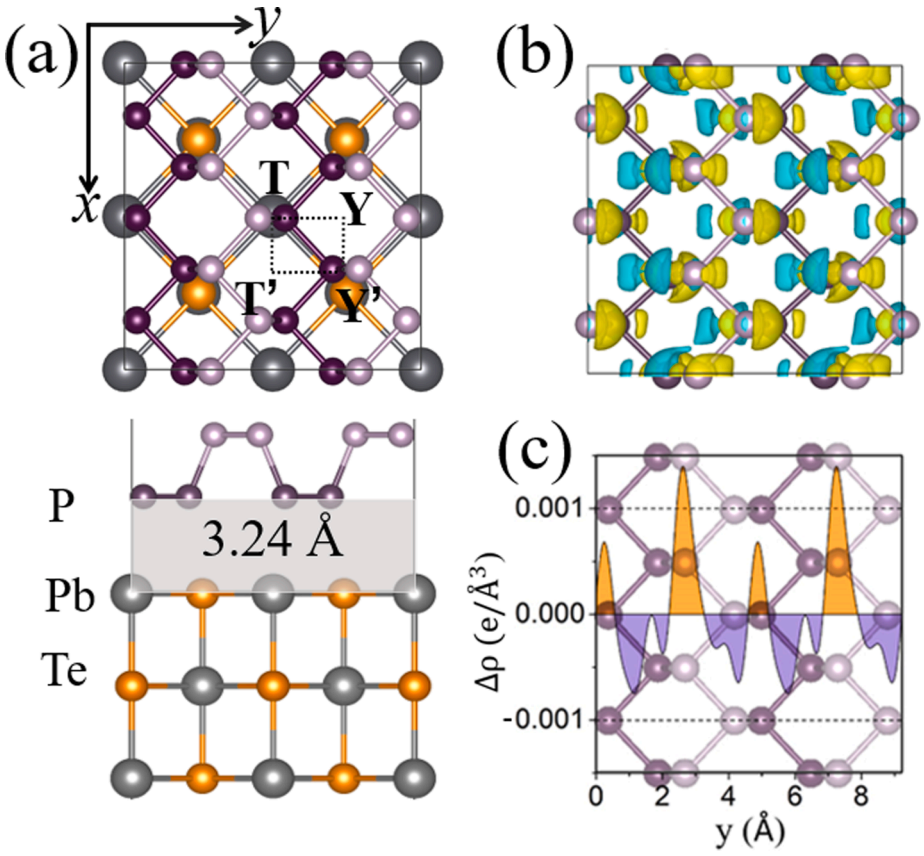

Fig. 2. (a) Top and side views of the P/PbTe vdW heterostructure. (b) Differential charge density of the monolayer phosphorene in the heterostructure with respect to intrinsic monolayer phosphorene without the substrate. Yellow and cyan colors represent charge accumulation and depletion. (c) The plane-averaged charge density difference $\Delta\rho$ along the y-direction. The positive and negative numbers represent charge accumulation and depletion. (For interpretation of the references to colour in this figure legend, the reader is referred to the web version of this article.)

heterostructure is less than 3%.

We now consider the symmetry structure of phosphorene on top of PbTe. The structure as shown in Fig. 2(a) has one of the P-P dimer on top of the Pb atom in the centre of the unit cell, and is labelled as T position of phosphorene on PbTe. Based on the symmetry of the P/PbTe heterostructure, a position shifting of phosphorene on PbTe to any other positions is energetically equivalent with a shifting to a position inside the rectangle indicated by the dashed lines. For the four corner positions of the rectangle in Fig. 2(a), T and T' (Y and Y') are symmetrically equivalent. The Y position can be deduced from the T position via sliding the phosphorene by half of the phosphorene unit cell along y axis (i.e. armchair direction). The two stacking positions have the same total energy due to the symmetry of P/PbTe, we choose the T position as a prototype in the following discussion.

To verify the stability of the P/PbTe vdW heterostructure, we calculated the binding energy of the heterostructure (E_b) as follows:

$$E_b = \frac{\left(E_{P/PbTe} - E_P - E_{PbTe}\right)}{n} \quad (1)$$

where $E_{P/PbTe}$ is the total energy of the P/PbTe vdW heterostructure, E_P and E_{PbTe} are the total energies of monolayer phosphorene and bulk PbTe, respectively, and n represents the number of atoms in the supercell of monolayer phosphorene. The binding energy as a function of interlayer distance is shown in Fig. S1, giving the lowest binding energy of −62 meV/atom at interlayer distance of 3.24 Å, which is in the same order of magnitude as in other vdW materials, suggesting the vdW interaction between phosphorene and PbTe substrate.

Fig. 2(b) shows the differential charge density of the monolayer phosphorene in the appearance of PbTe substrate with respect to that in the absence of substrate. The yellow and cyan colors represent charge accumulation and depletion. It can be seen clearly that the charge density is not symmetrically distributed on the P atoms when the PbTe substrate is applied. The reason can be seen from the side view of Fig. 2 (a). As the lower P-P dimmer bonds in puckered phosphorene lie on the Pb-Te bonds in PbTe, their uniformly distributed charge density is asymmetric now. As shown in Fig. 2(b), the positive charge centres and the negative charge centres of monolayer phosphorene are no longer coincident when the PbTe substrate is applied. Therefore, the monolayer phosphorene breaks its inherent inversion symmetry, in-plane rotational symmetry, and glide reflection symmetry between the two P sublattices in the appearance of PbTe substrate. Due to the above symmetry breaking's in phosphorene, the redistribution of electrons is asymmetrical on the two P sublattices, which drives the positive and negative charge centres apart from each other and renders an in-plane electric polarization in monolayer phosphorene. This asymmetrical charge density distribution is further confirmed by the plane-averaged charge density difference $\Delta\rho(y)$ along the y-direction in Fig. 2(c). Through Berry phase expression calculations, we estimate a 1.31 pC/m electric polarization for the distorted phosphorene structure as found in P/PbTe. For the T position of P/PbTe heterostructure, as shown in Fig. 2(a), the polarization direction is along the y direction, which is related to the non-symmetrical charge density distribution along the same direction, as shown in Fig. 2(c), illustrating that the two P sublattices that are inversion-symmetric with compensated local electric polarization in free standing phosphorene are not symmetrical with non-symmetrically distributed charge density in the heterostructure.

To further understand the electronic properties, we depict the projected band structure in Fig. 3(a), showing obvious characters of vdW interactions. Here, the green and pink solid lines denote the electronic states of phosphorene and PbTe separately. The P/PbTe vdW heterostructure behaves as a semiconductor with a direct band gap of 0.26 eV, similar with the bulk PbTe (~0.24 eV). The conduction band minimum (CBM) and the valence band maximum (VBM) lie at Γ. And it can be seen from Fig. 3(a) that the electronic state close to the Fermi level is completely contributed by the atomic orbitals of the substrate material PbTe, which indicates that the heterostructure has a type-I band alignment and the PbTe electronic states play a major role in the band edge properties of P/PbTe vdW heterostructure. Fig. 3(b) shows the band alignment of P/PbTe vdW heterostructure with vacuum level (E_{vacuum}) as the reference, further demonstrating the type-I band alignment of the heterostructure. The calculated energy band offsets of the P/PbTe heterostructure are $\Delta E_c = 0.35$ eV and $\Delta E_v = 0.24$ eV, respectively. While the natural band offsets between free standing phosphorene and PbTe are calculated to be $E_c = 0.024$ eV and $E_v = 0.73$ eV. The main cause of band deflection is the charge transfer between phosphorene and PbTe in the vdW heterostructure. Similar behaviour has been found in the h-BN/$MoSe_2$ system [50].

3.2. Modulating electric polarization by external fields

Modulating the physical and chemical properties of 2D nanomaterials is essential for various applications. Once the in-plane electric polarization is induced in phosphorene, we attempt to apply external fields to modulate/enhance it. The adiabatic path from the centrosymmetric paraelectric phase to the phosphorene on PbTe heterostructure allows us to calculate the total polarization using the modern polarization theory based on the Berry phase method. We investigated the effects of external strain and electric field on the induced in-plane electric polarization of phosphorene in P/PbTe. The strains are applied by changing the interlayer distance as deformation percentage $\varepsilon = -\frac{d-d_0}{d_0}$, where d and d_0 are the interlayer distance and equilibrium distance, respectively. Under zero electric field, the polarization varies with the interlayer strain greatly, from 1.31 to 9.39 pC/m for 0 to 25% deformation percentage. To check the dynamic stability of the heterostructure, we calculated the phonon band structure of the phosphorene in the heterostructure without and with 25% deformation percentage. We find no virtual frequency in the phonon spectrum, suggesting that the interface geometry is metastable for the heterostructure we considered as shown in Fig. S2. The increase of electric polarization induced by compressive strain can be rationalized in terms of the enhanced vdW interaction between phosphorene and PbTe under strain. Furthermore, it is found that although the in-plane polarization is induced by the PbTe substrate, the polarization value of the heterostructure in the z direction is small, much smaller than the in-plane polarization value.

An external electric field was further applied to modulate the in-plane electric polarization in the phosphorene on PbTe heterostructure. Many studies have shown that the use of an external electric field can effectively modulate the electronic properties of the

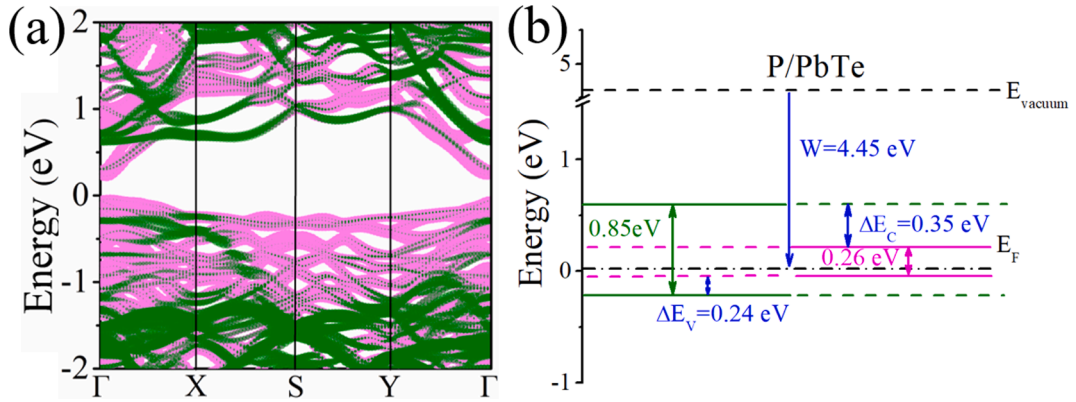

Fig. 3. (a) Projected band structure of the P/PbTe vdW heterostructure. (b) Band alignment of P/PbTe vdW. The bands dedicated by P and PbTe are highlighted by green and pink solid lines separately. The width of the lines represents the proportion of each material. (For interpretation of the references to colour in this figure legend, the reader is referred to the web version of this article.)

heterostructure [51–53] and has a prominent contribution to the ferroelectric polarization [20]. In our calculation, the external electric field is applied along the *z* direction with the electric potential decreases from the bottom of PbTe to the top of phosphorene (in the same direction of the vertical electric polarization of the pristine heterostructure). The magnitude of the applied electric field in our calculations is 0.5 V/Å, which has been experimentally implemented in two-dimensional materials [53]. We find that the in-plane polarization value of phosphorene in the heterostructure under 25% deformation percentage and $E_v = 0.5$ V/Å is around 12.29 pC/m (see Fig. S2 for the calculation process of the polarization value). This polarization value was roughly 50% larger than that of the case without an external electric field and almost ten times larger than the 1.31 pC/m without mechanical and electrical fields. For comparison, the in-plane polarization of phosphorene in the heterostructure without mechanical deformation is changed only by 0.02 pC/m under electrical field of 0.5 V/Å.

Fig. 4(a) shows the plane-averaged charge density difference Δρ along the *y*-direction under 25% deformation percentage, as compared to the Δρ under 25% deformation percentage and 0.5 V/Å electric field in Fig. 4(b). We see that Δρ in Fig. 4(b) is slightly larger than that in Fig. 4(a), which accounts for the increase of in-plane electric polarization under external electric field. The charge density difference Δρ in Fig. 4 (a) and (b) is about ten times larger than that in Fig. 2(c). This change of plane-averaged charge density difference obviously shows the modulation of electric polarization by interlayer strain and the external electric field. We also test the bilayer phosphorene on PbTe, the polarization value is almost the same with the monolayer. The reason is the in-plane electric polarization comes from the asymmetric charge distribution at the interface of P/PbTe vdW heterostructure rendered by PbTe substrate, which the layer number has no effect on.

3.3. Switching in-plane electric polarization

Next we evaluate the possibility to switch the in-plane electric polarization induced in phosphorene. Firstly, we performed electric polarization calculation for the Y structure (see Fig. 2(a)). This structure can be obtained by sliding of the phosphorene on the PbTe substrate, as illustrated in Fig. 2(a). When the phosphorene shifts along the armchair direction from T to Y, the former lower P-P dimmer bonds lying on Pb-Te bonds now change to lying on Te-Pb bonds. The local electric dipole field between the cation–anion (Pb-Te) chains attract the electrons of the lower P-P dimmer bond to the left (cation) side, leading to the asymmetric charge distribution on the two P sublattices as shown in Fig. 2(c), as well as the associated in-plane electric polarization. Whereas, the local field between the anion-cation (Te-Pb) chains attract the electrons to the right side and would lead to an in-plane polarization with the opposite direction to the case in Fig. 2(c). We used the Berry phase method to calculate the electric polarization of the T' and Y positions of the P/PbTe vdW heterostructure. Surely, it was found that when the monolayer phosphorene slides in the × direction with respect to the PbTe substrate, the direction and the value of the electric polarization will be almost the same compared with the T position of phosphorene on PbTe. However, when the phosphorene periodically slides in the *y* direction with respect to the PbTe substrate, the polarization direction would change periodically. For example, the direction of the in-plane polarization is reversed, but the calculated in-plane polarization value has almost the same magnitude, when the phosphorene slides from T to Y, which can be seen in Fig. S4 for the case of 25% deformation percentage (the plane-averaged charge density difference along the *y*-direction for Y position is shown in Fig. S5 that is sharply different than Fig. 4(a)). The periodic reversion of electric polarization is related to the periodic anion and cation chains in the PbTe substrate (see Fig. 2(a)). The periodic anion and cation chains in PbTe along × and *y* directions (Fig. 2(a)) are similar, whereas only the sliding of phosphorene along *y* direction but not along × direction leads to periodic sign change of polarization, which is related to the crystal structure and non-ferroelectric feature of phosphorene. As a mono-atomic analogue of the ferroelectric IV-VI monolayer with ferroelectric polarization along *y* (armchair) direction, free-standing phosphorene has the glide reflection plane perpendicular to the *y* direction, leading to the compensation of the electric polarizations along ± *y* directions of the two P sublattices. The appearance of the anion and cation chains in PbTe substrate breaks the compensation of the electric polarizations of the two P sublattices (distinguished by yellow plus signs in Fig. 1(a)), especially for the lower P layer (dark purple spheres in Fig. 1(a)). Furthermore, the T and Y heterostructures (see Fig. 2(a)) are connected by a glide reflection operation with the gliding reflection plane on the anion chain of PbTe surface perpendicular to *y* direction. Thus, the T and Y structures would possess identical total energy and opposite in-plane electric polarization directions with the same magnitude. Therefore, a type of electric polarization switching could be realized by the angstrom-scale shift of phosphorene on the PbTe substrate, without structural phase transformation in phosphorene.

We then evaluate the operability of the relative sliding of monolayer phosphorene and PbTe substrate. We calculated the energy migration barrier to be crossed between the two end-point structures, i.e. the T and Y positions (see Fig. 2(a)). The energy corresponding to the initial T structure is taken as the origin. We then compare the calculated total energies to obtain an estimated up-limit of the energy migration barrier by choosing three linear interpolation points between the initial and final structures. The results are shown in Fig. 5(a), giving an estimated energy barrier of 6.62 meV/P-atom that has certain operability in experiments (the energy migration barrier to be crossed between the T and T' positions in Fig. 2(a) is almost zero, as shown in Fig. S6, since T and T'

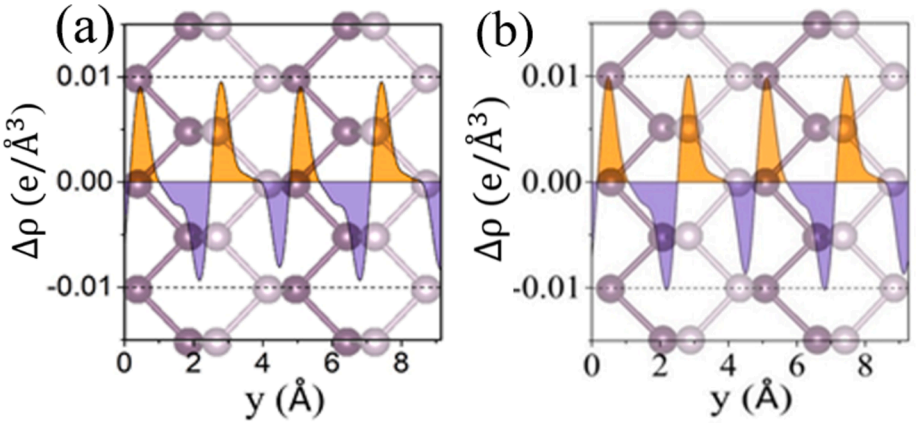

Fig. 4. (a, b) The plane-averaged charge density difference Δ*ρ* along the *y*-direction under 25% deformation percentage without (a) or with 0.5 V/Å electric field (b). The positive and negative numbers represent charge accumulation and depletion.

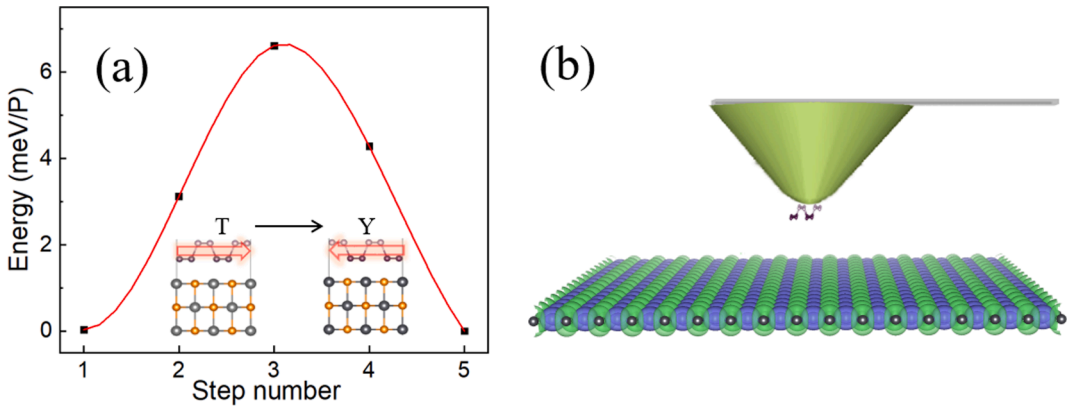

Fig. 5. (a) Energy barrier when phosphorene is shifting from T to Y position in the P/PbTe vdW heterostructure. The insets are the side view of the end-point structures. The red arrows denote the direction of electric polarizations in phosphorene. (b) Illustration of incorporation of phosphorene on the tip of STM system for the sensitivity on cation versus anion species of the substrate, analogous to the nickelocene-terminated tip that offers the possibility of producing spin excitations on the tip apex of STM [54]. (For interpretation of the references to colour in this figure legend, the reader is referred to the web version of this article.)

are identical with the same electric polarization), indicating that it is feasible to slide the monolayer phosphorene relative to the PbTe substrate. By calculating the total energies of an initial set of linear interpolation points of phosphorene positions on PbTe in the square indicated by dashed lines in Fig. 2(a), a 2D energy landscape could be fitted that can be used to suggest new position points for total energy calculations to improve the fitting, which eventually converges to suggest the lowest-energy electric polarization switching path in the 2D plane. Due to the strong anisotropic character of phosphorene (see e.g. the vanishing/finite linear migration barrier along *x/y* direction in Fig. S6 and Fig. 5(a)), the 2D migration barrier of phosphorene from T to Y positions on PbTe substrate would be similar to the that in Fig. 5(a). These results show that by choosing an appropriate substrate the phosphorene can be tuned to a material with easily-controllable electric polarization in atomic thickness.

For potential applications of the above discussed switchable electric polarization in P/PbTe heterostructure, as an atomic-scale spin sensing with a single molecule at the apex of a scanning tunneling micaroscope has been realize [54], we assume that one piece of phosphorene adsorbs on the tip of electronic microscope and slide on PbTe (or analogous materials with chains of cations and anions as illustrated in Fig. 5 (b)). If the phosphorene slides along its armchair direction, then the signal of tip will demonstrate a flip-flop electric polarization signal. From counting the number of flip-flop polarization signals, we can realize a precise distant measurement on the PbTe surface. We assume this can be used to further improve the precise distant control in modern scanning tunnel microscope or atomic force microscope. In the case of P/PbTe heterostructure as shown in Fig. 2(a), the ratio of the periodic *y* lattice dimensions of phosphorene and PbTe is 1:1. Based on the results discussed above, it is expected that for any ratio n:m with odd m as well as for incommensurate lattice dimensions (i.e. excluding only the exact ratio n:m with odd n and even m), there could also be an in-plane electric polarization due to the proximity of phosphorene to the substrate compound with alternating cation and anion chains along the armchair direction of phosphorene, which could also change sign when phosphorene slides on the substrate. For monolayer black arsenic [55,56] with optimized lattice constants $a = 3.69$ Å, $b = 4.76$ Å that is isostructural with phosphorene, we can construct a 5×2 supercell of black arsenic and a $2\sqrt{2} \times \sqrt{2}$ supercell of PbTe to form a black-arsenic/PbTe vdW heterostructure with a lattice mismatch of $\sim 3\%$, in which the ratio of the periodic *y* lattice dimensions of black-arsenic and PbTe is also 1:1. Furthermore, the vanishing/finite migration barrier along *x/y* direction in Fig. S6 and Fig. 5(a) coincides with the vanishing/finite in-plane electric polarization of phosphorene along *x/y* direction on PbTe, suggesting that an in-plane polarized phosphorene on an improper position on PbTe could raise the total energy of the system (by up to a few meV per P-atom). Therefore, it is possible to use lateral external electric field to change the relative energies of the different positions of phosphorene on PbTe, and trigger the shift of phosphorene to find a proper position that will generate in-plane electric polarization aligned with the electric field. Such in-plane electric polarization induced in 2D semiconductor phosphorene could be combined with the other optimal physical and chemical properties of phosphorene [13,14,17,18], opening the way of designing novel 2D electronic and optoelectronic devices.

4. Conclusions

In summary, we propose a type of in-plane polarization in phosphorene-based mixed dimensional heterostructure P/PbTe that can be switched via the sliding of phosphorene on PbTe substrate from cation to anion chains at angstrom-scale. The polarization magnitude in P/PbTe varies by up to ten times under vertical strain and external electric field with the maximum value of 12.29 pC/m. Our results suggest the route of inducing in-plane electric polarization in phosphorene and the approach of switching in-plane electric polarization via atomic-scale position shifting of phosphorene. With negligible changes of atomic bonds, the flip-flop electric polarization signals when phosphorene is shifting on the surface of substrate compound have potential applications in nanoelectronic devices. The above effects could also be found in vdW heterostructures based on other potential 2D materials such as black arsenic [55,56]. The approach of inducing in-plane electric polarization in 2D materials by vdW interactions could open new way of designing 2D based functional materials.

Funding

X.Z. acknowledges the support by the National Natural Science Foundation of China (No. 11774239) and Shenzhen Science and Technology Innovation Commission (Nos. JCYJ20170818093035338, KQTD20180412181422399, KQTD20170810105439418). The calculations were performed on the high performance computational centre of Zhengzhou University.

CRediT authorship contribution statement

Fei Wang: Conceptualization, Methodology, Writing - review & editing, Visualization. **Zhuang Ma:** Methodology, Visualization, Writing - review & editing. **Yuting Wei:** Methodology, Writing - original draft. **Pu Huang:** Methodology, Writing - review & editing. **Xiuwen Zhang:** Conceptualization, Methodology, Writing - review & editing,

Visualization, Supervision.

Declaration of Competing Interest

The authors declare that they have no known competing financial interests or personal relationships that could have appeared to influence the work reported in this paper.

Appendix A. Supplementary material

Supplementary data to this article can be found online at https://doi.org/10.1016/j.apsusc.2021.150276.

References

[1] L.W. Martin, A.M. Rappe, Thin-film ferroelectric materials and their applications, Nat. Rev. Mater. 2 (2017) 16087, https://doi.org/10.1038/natrevmats.2016.87.
[2] J.F. Scott, Applications of modern ferroelectrics, Science. 315 (2007) 954–959, https://doi.org/10.1126/science.1129564.
[3] K. Liu, J. Lu, S. Picozzi, L. Bellaiche, H. Xiang, Intrinsic origin of enhancement of ferroelectricity in SnTe ultrathin films, Phys. Rev. Lett. 121 (2018) 27601, https://doi.org/10.1103/PhysRevLett.121.027601.
[4] F. Liu, L. You, K.L. Seyler, X. Li, P. Yu, J. Lin, X. Wang, J. Zhou, H. Wang, H. He, S. T. Pantelides, W. Zhou, P. Sharma, X. Xu, P.M. Ajayan, J. Wang, Z. Liu, Room-temperature ferroelectricity in CuInP2S6 ultrathin flakes, Nat. Commun. 7 (2016) 12357, https://doi.org/10.1038/ncomms12357.
[5] S. Shen, C. Liu, Y. Ma, B. Huang, Y. Dai, Robust two-dimensional ferroelectricity in single-layer γ-SbP and γ-SbAs, Nanoscale. 11 (2019) 11864–11871, https://doi.org/10.1039/c9nr02265a.
[6] Z. Fei, W. Zhao, T.A. Palomaki, B. Sun, M.K. Miller, Z. Zhao, J. Yan, X. Xu, D. H. Cobden, Ferroelectric switching of a two-dimensional metal, Nature. 560 (2018) 336–339, https://doi.org/10.1038/s41586-018-0336-3.
[7] M. Wu, P. Jena, The rise of two-dimensional van der Waals ferroelectrics, Wiley Interdiscip. Rev. Comput. Mol. Sci. 8 (2018), e1365, https://doi.org/10.1002/wcms.1365.
[8] Z. Guan, H. Hu, X. Shen, P. Xiang, N. Zhong, J. Chu, C. Duan, Recent progress in two-dimensional ferroelectric materials, Adv. Electron. Mater. 6 (2020) 1900818, https://doi.org/10.1002/aelm.201900818.
[9] H. Wang, X. Qian, Two-dimensional multiferroics in monolayer group IV monochalcogenides, 2D Mater. 4 (2017), 015042, https://doi.org/10.1088/2053-1583/4/1/015042.
[10] M. Wu, X.C. Zeng, Intrinsic ferroelasticity and/or multiferroicity in two-dimensional phosphorene and phosphorene analogues, Nano Lett. 16 (2016) 3236–3241, https://doi.org/10.1021/acs.nanolett.6b00726.
[11] R. Fei, W. Kang, L. Yang, Ferroelectricity and phase transitions in monolayer group-IV monochalcogenides, Phys. Rev. Lett. 117 (2016), 097601, https://doi.org/10.1103/PhysRevLett.117.097601.
[12] K. Chang, J. Liu, H. Lin, N. Wang, K. Zhao, A. Zhang, F. Jin, Y. Zhong, X. Hu, W. Duan, Q. Zhang, L. Fu, Q.-K. Xue, X. Chen, S.-H. Ji, Discovery of robust in-plane ferroelectricity in atomic-thick SnTe, Science. 353 (2016) 274–278, https://doi.org/10.1126/science.aad8609.
[13] L. Li, Y. Yu, G.J. Ye, Q. Ge, X. Ou, H. Wu, D. Feng, X.H. Chen, Y. Zhang, Black phosphorus field-effect transistors, Nat. Nanotechnol. 9 (2014) 372–377, https://doi.org/10.1038/nnano.2014.35.
[14] Z. Guo, H. Zhang, S. Lu, Z. Wang, S. Tang, J. Shao, Z. Sun, H. Xie, H. Wang, X.F. Yu, P.K. Chu, From black phosphorus to phosphorene: basic solvent exfoliation, evolution of raman scattering, and applications to ultrafast photonics, Adv. Funct. Mater. 25 (2015) 6996–7002, https://doi.org/10.1002/adfm.201502902.
[15] A.K. Geim, K.S. Novoselov, The rise of graphene, Nat. Mater. 6 (2007) 183–191, https://doi.org/10.1038/nmat1849.
[16] K.S. Novoselov, Electric field effect in atomically thin carbon films, Science. 306 (2004) 666–669, https://doi.org/10.1126/science.1102896.
[17] L. Li, J. Kim, C. Jin, G.J. Ye, D.Y. Qiu, F.H. Da Jornada, Z. Shi, L. Chen, Z. Zhang, F. Yang, K. Watanabe, T. Taniguchi, W. Ren, S.G. Louie, X.H. Chen, Y. Zhang, F. Wang, Direct observation of the layer-dependent electronic structure in phosphorene, Nat. Nanotechnol. 12 (2017) 21–25, https://doi.org/10.1038/nnano.2016.171.
[18] F. Xia, H. Wang, Y. Jia, Rediscovering black phosphorus as an anisotropic layered material for optoelectronics and electronics, Nat. Commun. 5 (2014) 4458, https://doi.org/10.1038/ncomms5458.
[19] X. Zhang, Q. Liu, J.W. Luo, A.J. Freeman, A. Zunger, Hidden spin polarization in inversion-symmetric bulk crystals, Nat. Phys. 10 (2014) 387–393, https://doi.org/10.1038/nphys2933.
[20] T. Hu, H. Wu, H. Zeng, K. Deng, E. Kan, New ferroelectric phase in atomic-thick phosphorene nanoribbons: existence of in-plane electric polarization, Nano Lett. 16 (2016) 8015–8020, https://doi.org/10.1021/acs.nanolett.6b04630.
[21] K.S. Novoselov, A. Mishchenko, A. Carvalho, A.H. Castro Neto, 2D materials and van der Waals heterostructures, Science. 353 (2016) aac9439, https://doi.org/10.1126/science.aac9439.
[22] X. Wang, F. Xia, Stacked 2D materials shed light, Nat. Mater. 14 (2015) 264–265, https://doi.org/10.1038/nmat4218.
[23] X. Zhou, X. Hu, J. Yu, S. Liu, Z. Shu, Q. Zhang, H. Li, Y. Ma, H. Xu, T. Zhai, 2D layered material-based van der waals heterostructures for optoelectronics, Adv. Funct. Mater. 28 (2018) 1706587, https://doi.org/10.1002/adfm.201706587.
[24] P. Ajayan, P. Kim, K. Banerjee, Two-dimensional van der Waals materials, Phys. Today. 69 (2016) 38–44, https://doi.org/10.1063/PT.3.3297.
[25] Y. Fan, M. Zhao, Z. Wang, X. Zhang, H. Zhang, Tunable electronic structures of graphene/boron nitride heterobilayers, Appl. Phys. Lett. 98 (2011), 083103, https://doi.org/10.1063/1.3556640.
[26] A. Mishchenko, J.S. Tu, Y. Cao, R. V Gorbachev, J.R. Wallbank, M.T. Greenaway, V.E. Morozov, S. V Morozov, M.J. Zhu, S.L. Wong, F. Withers, C.R. Woods, Y. Kim, K. Watanabe, T. Taniguchi, E.E. Vdovin, O. Makarovsky, T.M. Fromhold, V.I. Fal'ko, A.K. Geim, L. Eaves, K.S. Novoselov, Twist-controlled resonant tunnelling in graphene/boron nitride/graphene heterostructures, Nat. Nanotechnol. 9 (2014) 808–813. https://doi.org/10.1038/nnano.2014.187.
[27] Y. Deng, Z. Luo, N.J. Conrad, H. Liu, Y. Gong, S. Najmaei, P.M. Ajayan, J. Lou, X. Xu, P.D. Ye, Black phosphorus-monolayer MoS 2 van der Waals heterojunction p–n diode, ACS Nano. 8 (2014) 8292–8299, https://doi.org/10.1021/nn5027388.
[28] W.J. Yu, Y. Liu, H. Zhou, A. Yin, Z. Li, Y. Huang, X. Duan, Highly efficient gate-tunable photocurrent generation in vertical heterostructures of layered materials, Nat. Nanotechnol. 8 (2013) 952–958, https://doi.org/10.1038/nnano.2013.219.
[29] W.J. Yu, Q.A. Vu, H. Oh, H.G. Nam, H. Zhou, S. Cha, J.-Y. Kim, A. Carvalho, M. Jeong, H. Choi, A.H. Castro Neto, Y.H. Lee, X. Duan, Unusually efficient photocurrent extraction in monolayer van der Waals heterostructure by tunnelling through discretized barriers, Nat. Commun. 7 (2016) 13278, https://doi.org/10.1038/ncomms13278.
[30] D. Jariwala, T.J. Marks, M.C. Hersam, Mixed-dimensional van der Waals heterostructures, Nat. Mater. 16 (2017) 170–181, https://doi.org/10.1038/nmat4703.
[31] Y. Sun, W. Zhong, Y. Wang, X. Xu, T. Wang, L. Wu, Y. Du, MoS2 -based mixed-dimensional van der Waals heterostructures: A new platform for excellent and controllable microwave-absorption performance, ACS Appl. Mater. Interfaces. 9 (2017) 34243–34255, https://doi.org/10.1021/acsami.7b10114.
[32] D. Schwarz, Y. Noda, J. Klouda, K. Schwarzová-Pecková, J. Tarábek, J. Rybáček, J. Janoušek, F. Simon, M.V. Opanasenko, J. Čejka, A. Acharjya, J. Schmidt, S. Selve, V. Reiter-Scherer, N. Severin, J.P. Rabe, P. Ecorchard, J. He, M. Polozij, P. Nachtigall, M.J. Bojdys, Twinned growth of metal-free, triazine-based photocatalyst films as mixed-dimensional (2D/3D) van der Waals heterostructures, Adv. Mater. 29 (2017) 1703399, https://doi.org/10.1002/adma.201703399.
[33] R. Zhuo, L. Zeng, H. Yuan, D. Wu, Y. Wang, Z. Shi, T. Xu, Y. Tian, X. Li, Y.H. Tsang, In-situ fabrication of PtSe2/GaN heterojunction for self-powered deep ultraviolet photodetector with ultrahigh current on/off ratio and detectivity, Nano Res. 12 (2019) 183–189, https://doi.org/10.1007/s12274-018-2200-z.
[34] H. Ra, D. Kwak, J. Lee, A hybrid MoS2 nanosheet–CdSe nanocrystal phototransistor with a fast photoresponse, Nanoscale. 8 (2016) 17223–17230, https://doi.org/10.1039/C6NR05393A.
[35] D. Kufer, I. Nikitskiy, T. Lasanta, G. Navickaite, F.H.L. Koppens, G. Konstantatos, Hybrid 2D–0D MoS 2 -PbS Quantum Dot Photodetectors, Adv. Mater. 27 (2015) 176–180, https://doi.org/10.1002/adma.201402471.
[36] D. Ruzmetov, K. Zhang, G. Stan, B. Kalanyan, G.R. Bhimanapati, S.M. Eichfeld, R. A. Burke, P.B. Shah, T.P. O'Regan, F.J. Crowne, A.G. Birdwell, J.A. Robinson, A. V. Davydov, T.G. Ivanov, Vertical 2D/3D Semiconductor Heterostructures Based on Epitaxial Molybdenum Disulfide and Gallium Nitride, ACS Nano. 10 (2016) 3580–3588, https://doi.org/10.1021/acsnano.5b08008.
[37] G. Kresse, J. Furthmüller, Efficient iterative schemes for ab initio total-energy calculations using a plane-wave basis set, Phys. Rev. B. 54 (1996) 11169–11186, https://doi.org/10.1103/PhysRevB.54.11169.
[38] G. Kresse, J. Furthmüller, Efficiency of ab-initio total energy calculations for metals and semiconductors using a plane-wave basis set, Comput. Mater. Sci. 6 (1996) 15–50, https://doi.org/10.1016/0927-0256(96)00008-0.
[39] P.E. Blöchl, Projector augmented-wave method, Phys. Rev. B. 50 (1994) 17953–17979, https://doi.org/10.1103/PhysRevB.50.17953.
[40] G. Kresse, D. Joubert, From ultrasoft pseudopotentials to the projector augmented-wave method, Phys. Rev. B. 59 (1999) 1758–1775, https://doi.org/10.1103/PhysRevB.59.1758.
[41] J.P. Perdew, K. Burke, M. Ernzerhof, Generalized gradient approximation made simple, Phys. Rev. Lett. 77 (1996) 3865–3868, https://doi.org/10.1103/PhysRevLett.77.3865.
[42] H.J. Monkhorst, J.D. Pack, Special points for Brillouin-zone integrations, Phys. Rev. B. 13 (1976) 5188–5192, https://doi.org/10.1103/PhysRevB.13.5188.
[43] A. Togo, L. Chaput, I. Tanaka, G. Hug, First-principles phonon calculations of thermal expansion in Ti3SiC2, Ti3AlC2, and Ti3GeC2, Phys. Rev. B. 81 (2010), 174301, https://doi.org/10.1103/PhysRevB.81.174301.
[44] A. Togo, I. Tanaka, First principles phonon calculations in materials science, Scr. Mater. 108 (2015) 1–5, https://doi.org/10.1016/j.scriptamat.2015.07.021.
[45] R.D. King-Smith, D. Vanderbilt, Theory of polarization of crystalline solids, Phys. Rev. B. 47 (1993) 1651–1654, https://doi.org/10.1103/PhysRevB.47.1651.
[46] R. Resta, D. Vanderbilt, Chapter 02 Theory of Polarization: A Modern Approach, in: Phys. Ferroelectr., Springer-Verlag Berlin Heidelberg, 2007: pp. 31–68. https://doi.org/10.1007/978-3-540-34591-6_2.
[47] N.A. Spaldin, A beginners guide to the modern theory of polarization, J. Solid State Chem. 195 (2012) 2–10, https://doi.org/10.1016/j.jssc.2012.05.010.
[48] G. Henkelman, B.P. Uberuaga, H. Jónsson, A climbing image nudged elastic band method for finding saddle points and minimum energy paths, J. Chem. Phys. 113 (2000) 9901–9904, https://doi.org/10.1063/1.1329672.

[49] W. Yu, Z. Zhu, C. Niu, C. Li, J. Cho, Y. Jia, Anomalous doping effect in black phosphorene using first-principles calculations, Phys. Chem. Chem. Phys. 17 (2015) 16351–16358, https://doi.org/10.1039/C5CP01732G.
[50] D.S. Koda, F. Bechstedt, M. Marques, L.K. Teles, Coincidence Lattices and Interlayer Twist in van der Waals Heterostructures: Application of the Coincidence Lattice Method on hBN/MoSe2 Heterobilayer Systems, J. Electron. Mater. 46 (2017) 3910–3916, https://doi.org/10.1007/s11664-016-5037-9.
[51] C. Xia, J. Du, M. Li, X. Li, X. Zhao, T. Wang, J. Li, Effects of electric field on the electronic structures of broken-gap phosphorene/SnX2 van der Waals heterojunctions, Phys. Rev. Appl. 10 (2018), 054064, https://doi.org/10.1103/PhysRevApplied.10.054064.
[52] Y. Wei, F. Wang, W. Zhang, X. Zhang, The electric field modulation of electronic properties in a type-II phosphorene/PbI 2 van der Waals heterojunction, Phys. Chem. Chem. Phys. 21 (2019) 7765–7772, https://doi.org/10.1039/C9CP00733D.
[53] Y. Zhang, T. Tang, C. Girit, Z. Hao, M.C. Martin, A. Zettl, M.F. Crommie, Y.R. Shen, F. Wang, Direct observation of a widely tunable bandgap in bilayer graphene, Nature. 459 (2009) 820–823, https://doi.org/10.1038/nature08105.
[54] B. Verlhac, N. Bachellier, L. Garnier, M. Ormaza, P. Abufager, R. Robles, M. L. Bocquet, M. Ternes, N. Lorente, L. Limot, Atomic-scale spin sensing with a single molecule at the apex of a scanning tunneling microscope, Science. 366 (2019) 623–627, https://doi.org/10.1126/science.aax8222.
[55] Y. Chen, C. Chen, R. Kealhofer, H. Liu, Z. Yuan, L. Jiang, J. Suh, J. Park, C. Ko, H. S. Choe, J. Avila, M. Zhong, Z. Wei, J. Li, S. Li, H. Gao, Y. Liu, J. Analytis, Q. Xia, M. C. Asensio, J. Wu, Black Arsenic: A layered semiconductor with extreme in-plane anisotropy, Adv. Mater. 30 (2018) 1800754, https://doi.org/10.1002/adma.201800754.
[56] M. Zhong, Q. Xia, L. Pan, Y. Liu, Y. Chen, H.-X. Deng, J. Li, Z. Wei, Thickness-dependent carrier transport characteristics of a New 2D elemental semiconductor: black arsenic, Adv. Funct. Mater. 28 (2018) 1802581, https://doi.org/10.1002/adfm.201802581.